

# Modeling Nonlinear Plasma Formation for Femtosecond Processing of Transparent Materials and Biological Cells at High NA Focusing

Cord L. Arnold, Alexander Heisterkamp, Holger Lubatschowski

*Laser Zentrum Hannover e.V., Hollerithallee 8, 30419 Hannover, Germany  
E-mail: C.Arnold@lzh.de*

Ultrashort laser pulses recently found extensive application in micro- and nanostructuring, in refractive surgery of the eye, and in biophotonics. Due to the high laser intensity required to induce optical breakdown, nonlinear plasma formation is generally accompanied by a number of undesired nonlinear side-effects such as self-focusing, filamentation and plasma-defocusing, seriously limiting achievable precision and reproducibility. To reduce pulse energy, enhance precision, and limit nonlinear side effects, applications of ultrashort pulses have recently evolved towards tight focusing using high numerical aperture microscope objectives. However, from the theoretical and numerical point of view, generation of optical breakdown at high numerical aperture focusing was barely studied.

To simulate the interaction of ultrashort laser pulses with transparent materials at high NA focusing, a comprehensive numerical model was introduced by the authors in [1], taking into account nonlinear propagation, plasma generation as well as the pulse's interaction with the generated plasma. The multiple rate equation (MRE) model [2] is used to simultaneously calculate the generation of free electrons. Nonparaxial and vectorial diffraction theory provides initial conditions. The theoretical model derived in [1] is applied to numerically study the generation of optical breakdown plasmas, concentrating on parameters usually found in experimental applications of cell surgery. Water is used as a model substance for biological soft tissue and cellular constituents. For focusing conditions of low to moderate numerical aperture ( $NA < 0.9$ ) generation of optical breakdown is shown to be strongly influenced by plasma defocusing, resulting in spatially distorted breakdown plasmas of expanded size. For focusing conditions of high numerical aperture ( $NA \geq 0.9$ ) on the other hand generation of optical breakdown is found to be almost unaffected by distortive side-effects, perfectly suited for material manipulation of highest precision.

**Keywords:** Ultrashort Laser Pulses, Optical Breakdown, Nonlinear Pulse Propagation, Nonlinear Ionization, Nanosurgery, Nonparaxial and Vectorial Optics

## 1. Introduction

The possibility to manipulate transparent materials by focused ultrashort laser pulses has recently attracted a multitude of potential and well established applications. Among these are micro- and nanomachining of transparent materials for e.g. generation of waveguides [3] or micro fluidic elements [4]. Ultrashort pulse emitting lasers are now commercially used for the generation of the flap as part of the well known LASIK (laser in situ keratomileusis) procedure for ametropia correction [5, 6]. Ultrashort pulses also proved valuable for multiphoton imaging and nanosurgery of biological cells and micro organisms [7-10]. All of the aforementioned applications are based on nonlinear interaction of focused ultrashort laser pulses with a particular material. The manipulability is due to the generation of a dense electron-hole plasma via nonlinear ionization processes. If the density of generated free electrons and thus the energy deposited in the focal volume is sufficient to alter the material, the process is termed optical breakdown. For solid state materials such as glasses the alteration can either be local melting followed by solidification as used for writing waveguides [11] or local shivering resulting in the gen-

eration of cavities inside the material [12]. In aqueous media like water or biological soft tissue optical breakdown results in the generation of a cavitation bubble expanding from the focus and disrupting the adjacent material. This process is often termed photodisruption.

In addition to the generation of optical breakdown the interaction of ultrashort laser pulses with transparent materials bares a multitude of other nonlinear effects, such as self-focusing, self-phase modulation, filamentation, and supercontinuum generation. The actual mode of nonlinear interaction is a function of many parameters such as peak power, intensity, pulse duration, and external focusing. The generation of optical breakdown generally competes with nonlinear propagation effects. At loose external focusing filamentation and supercontinuum generation are more likely to occur than optical breakdown [13, 14]. In addition optical breakdown can be accompanied by streak formation [12, 15-17]. Streak-formation is mainly due to the spatio-temporal asymmetric interaction of the pulse with the generated plasma [15]. Filamentation and streak formation generate non negligible free electron density apart the very focus and thus enlarge and distort the volume of interaction.

These effects are therefore of parasitic nature to applications utilizing ultrashort laser pulses to precisely and reproducibly manipulate materials via the generation of optical breakdown [12, 18]. Experimentally it is a well known fact that the intensity of these parasitic side-effects decreases as external focusing increases. Hence applications of ultrashort pulses recently evolved towards tight focusing at high numerical aperture to reduce pulse energy, enhance precision, and limit nonlinear side effects. Exemplary are applications in nanomachining of materials as well as cell surgery [19].

There is a multitude of publications concerning numerical modeling of the interaction of ultrashort laser pulses with the bulk of transparent materials at low to medium numerical aperture [15-17, 20-21]. Aspects that are of importance at high numerical aperture, such as nonparaxiality and vectorial effects were only partially considered before [22-26], but mainly as possible processes to arrest catastrophic self-focusing, which limits the use of simple nonlinear Schrödinger equation approaches [27]. A theoretical model to study the nonlinear interaction taking into account both nonlinear pulse propagation and nonlinear plasma formation at strong spatial focusing was presented by the authors in a previous paper [1]. The model is especially suited to meet experimental conditions as found in modern applications using microscope objectives to focus ultrashort pulses to diffraction limited spot size for nanomachining and cell surgery.

The objective of the work presented is to theoretically and numerically study the generation of optical breakdown at high NA focusing. Since any modification, whether of thermal or mechanical nature, induced in the material is a direct result of the plasma generated in the focus, the size, the shape, and the density of the plasma is of particular interest. Possible parasitic side-effects enlarge and distort the shape of the generated plasma, resulting in an increased breakdown threshold energy and limiting the precision achievable in a particular application. The numerical model is based on a nonlinear propagation equation which was derived in a general manner and subsequently carefully adapted to particularly suit high NA focusing. Plasma generation via nonlinear photo ionization and cascade ionization is calculated using the multiple rate equation (MRE) model [2]. The propagation equation is coupled to the MRE model by the complex susceptibility function of the ionized material. Providing the focal laser field as initial conditions for the nonlinear calculation is a crucial point at tight focusing. A nonparaxial diffraction integral was vectorially expanded to account for xy-asymmetries and depolarization effects apparent at tight focusing [28-30].

We concentrate on parameters usually found in applications of cell surgery. Since data on the nonlinear properties of biological materials is generally not available, liquid water is used here as a model substance for cellular constituents. It was shown before that the breakdown threshold in water is very similar to that in biological media [31]. Water can in good approximation be treated as an amorphous semiconductor with a bandgap energy of  $\Delta = 6.5$  eV [32]. The commonly accepted criterion for optical breakdown of  $\rho_{Bd} = 10^{21}$  cm<sup>-3</sup> generated free electrons [33] is applied within this work. This corresponds to an energy density of about 1.8 kJcm<sup>-3</sup> deposited in focus.

There are two different methods commonly used for femtosecond laser nanoprocessing of biomaterials [33]. In this work the generation of optical breakdown is assumed to be induced by single pulses. The dissection of material subsequent to optical breakdown relies on thermoelastically induced formation of cavitation bubbles. This is generally the case, when either single pulses or kHz repetition rates are experimentally used. The second method uses long trains of oscillator pulses of high repetition rate, usually 80 MHz, and pulse energy well below the optical breakdown threshold of a single pulse. The dissection is mediated by free-electron-induced chemical decomposition [33]. However, this regime would require a totally different theoretical approach as used here.

## 2. Theoretical Model

The theoretical model used to numerically study the interaction of ultrashort laser pulses with transparent materials at high numerical aperture was described in detail in an earlier publication [1]. For the general case that incoming ultrashort laser pulses are linearly polarized before being focused into the sample, it was shown before that numerically treating the transverse polarization direction only is sufficient to grasp the general vectorial character of nonlinear propagation [1, 25, 34]. Starting with the vectorial Helmholtz equation a nonlinear, unidirectional propagation equation was derived in [1], to numerically treat the transverse field amplitude of ultrashort laser pulses being focused inside the bulk of transparent materials at high numerical aperture. Unlike the derivation of popular nonlinear propagation equations, the scalar and paraxial approximations were not applied. These approximations generally considerably simplify the equations yielded, but at the same time restrict the validity to the case of low numerical aperture. Contrary, in [1] the propagation equation was expanded by means of a small parameter  $f$ , which scales with the numerical aperture of the focusing objective ( $f \approx 2NA/\pi n_0$ ). Here  $n_0$  is the refractive index of the particular material. The parameter  $f$  is used to introduce specific simplifications and approximations for a given numerical aperture.

The nonlinear interaction of focused ultrashort laser pulses with a particular material is numerically mediated by a nonlinear susceptibility function  $\chi_{fe}$ , taking into account the Kerr effect, as well as the refractive and absorptive effects of free electrons generated by nonlinear ionization. Propagation effects incorporated in the susceptibility function  $\chi_{fe}$  are thus self-focusing, plasma defocusing, and plasma absorption. The generation of free electrons is numerically treated using the multiple rate equation (MRE) model [2].

As the intensity in the focus grows sufficiently high, electrons are initially transferred from the valence band to the energetic bottom of the conduction band via multiphoton or tunnel ionization. Once in the conduction band, electrons can climb a virtual energy ladder by sequential one-photon absorption, often also termed absorption of inverse bremsstrahlung. When the kinetic energy of free electrons exceeds the critical energy  $\epsilon_{crit}$ , additional electrons can be transferred to the conduction band via impact

ionization of atoms or molecules. The combination of sequential one-photon absorption and subsequent impact ionization is termed cascade or avalanche ionization. The main processes contributing to nonlinear plasma generation are depicted in fig. (1).

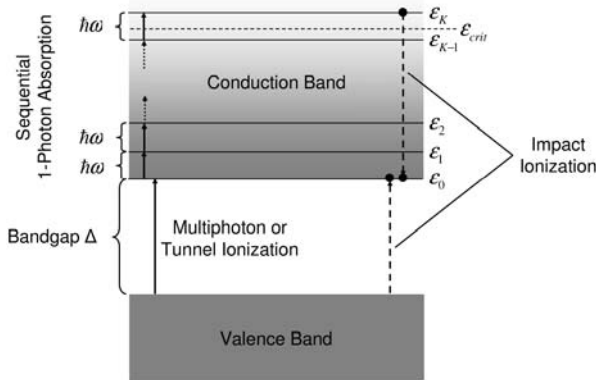


**Fig. 1** Nonlinear ionization processes in dielectrics, illuminated by high intensity ultrashort laser pulses.

Each virtual energy level in the conduction band is described by one rate equation in the MRE model. The MRE model keeps track of the fast temporal dynamics in the conduction band for ultrashort pulse nonlinear ionization. By contrast the simpler Drude model [35, 36], commonly used to account for nonlinear ionization, tends to overestimate the influence of cascade ionization for ultrashort pulses [2, 37]. Due to the lack of knowledge of the impact ionization probability  $W_{\text{Imp}}(\epsilon)$  for an electron in the conduction band with kinetic energy greater than  $\epsilon_{\text{crit}}$ , the MRE model was slightly simplified here by assuming instantaneous impact ionization, once  $\epsilon_{\text{crit}}$  is exceeded. The system of rate equations reads:

$$\begin{aligned} \frac{\partial \rho_0(t)}{\partial t} &= W_{\text{PI}}(I(t)) - W_{\text{IP}_1}(I(t))\rho_0(t) + 2W_{\text{IP}_1}(I(t))\rho_{K-1}(t) \\ \frac{\partial \rho_1(t)}{\partial t} &= W_{\text{IP}_1}(I(t))\rho_0(t) - W_{\text{IP}_1}(I(t))\rho_1(t) \\ &\vdots \\ \frac{\partial \rho_{K-1}(t)}{\partial t} &= W_{\text{IP}_1}(I(t))\rho_{K-2}(t) - W_{\text{IP}_1}(I(t))\rho_{K-1}(t) \end{aligned} \quad (1)$$

The rate for nonlinear photo ionization  $W_{\text{PI}}(I(t))$ , where  $I$  is the laser intensity, is calculated from the Keldysh theory [38]. The one-photon-absorption probability  $W_{\text{PI}}(I(t))$  is derived from the Drude model, assuming that the MRE and the Drude model result in the same ionization rate for long pulses [2].

Since the propagation equation used is nonparaxial and takes into account vectorial effects, initial focal fields must also be provided in a nonparaxial and vectorial manner. Focal fields are thus calculated using a FFT-based, nonparaxial variation of the Fresnel-Kirchhoff diffraction integral [29], which was vectorially expanded to account for high NA microscope objectives. As a result of tight focusing, strong depolarization and focal xy-asymmetries occur [28, 30, 39]. In order to calculate the vectorial light field in the focal plane, each polarization direction is de-

finied relative to a reference sphere (fig. 2). Subsequently a nonparaxial diffraction integral is performed for each polarization direction. The initial polarization direction was arbitrarily chosen to be the x-direction.

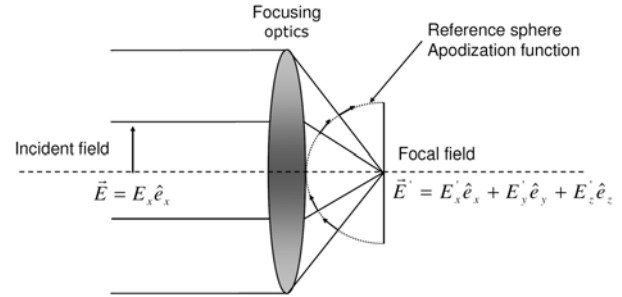


**Fig. 2** An ideal focusing optics transfers incoming plane waves into spherically converging waves. A nonparaxial diffraction integral transforms each polarization direction to the focus. The focal vector field is obtained by summing the components.

Unless phase errors from the beam itself or from the focusing optics are included, the wave front is flat on the reference sphere. The focal transversal fluence distribution is shown in fig. (3) for a numerical aperture  $\text{NA} = 1.2$  in water. The sine condition, which is usually the obeyed condition for the design of commercial objectives, was used as apodization function [29]. Depolarization results in 20.4 % of total beam power being polarized along the axial direction, 78.5 % remain linearly x-polarized. The remaining 1.1 % transferred in the y-polarization direction are neglected for the modeling. A distinct xy-asymmetry due to tight focusing can be observed in fig. (3) for both the x-, and the z-polarization direction, as well as for the vectorial fluence distribution.

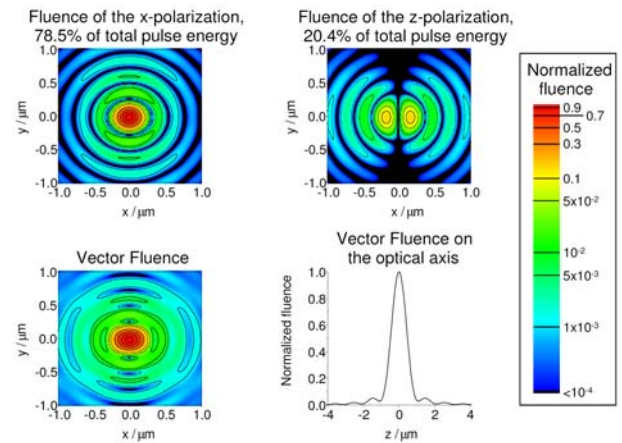
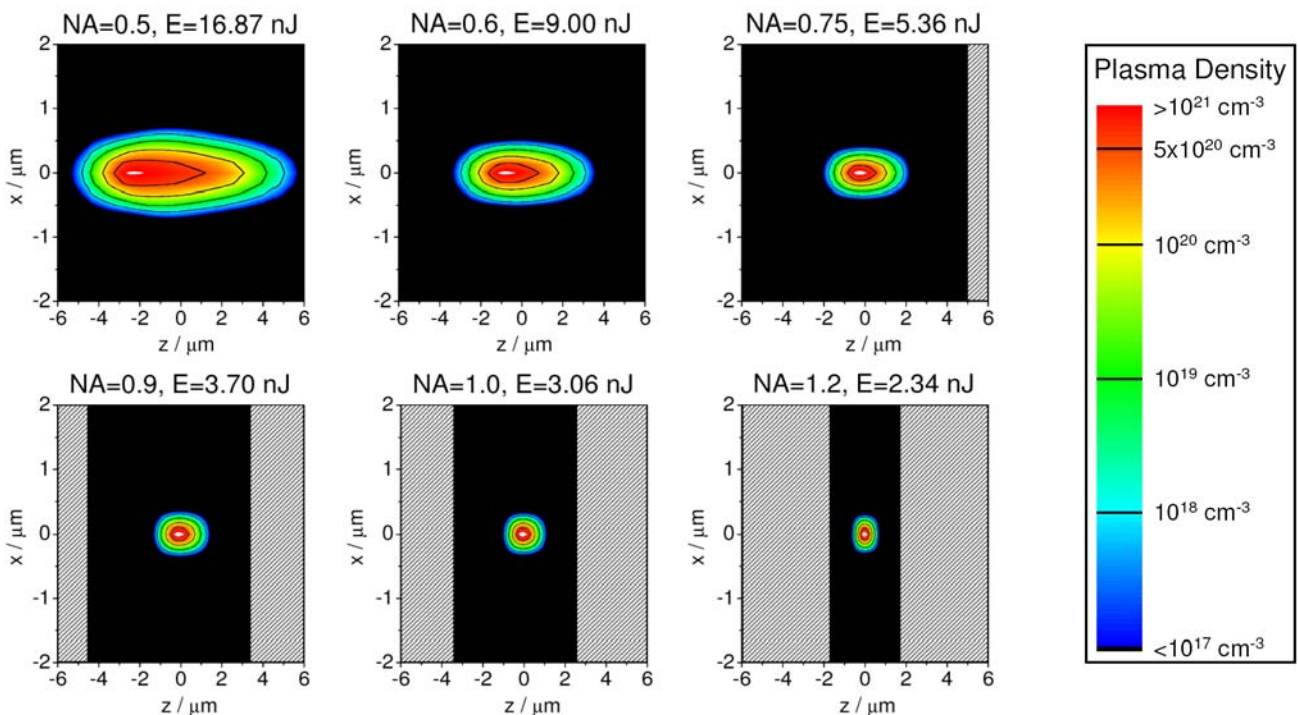


**Fig. 3** Focal Fluence distributions for numerical aperture  $\text{NA} = 1.2$  in water. The plots are normalized to the maximum fluence at the origin, the color scaling is logarithmic and the contour lines are at the levels:  $F = 0.9, 0.7, 0.5, 0.3, 0.1, 0.05, 0.01, 0.005, 0.001 F_0$ .

### 3. Results and Discussion

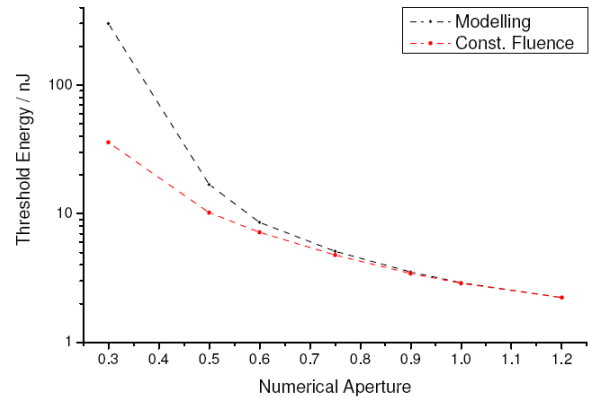
The theoretical model presented was applied to numerically simulate the generation of optical breakdown for focusing conditions of medium to high numerical aperture ( $0.5 \leq NA \leq 1.2$ ). The parameters were chosen to correspond to conditions as typically found in cell surgery and related applications. Ultrashort pulses were assumed to have  $\tau_0 = 150$  fs (FWHM) transform limited pulse duration, centred at  $\lambda = 780$  nm. For the highest  $NA = 1.2$  considered the threshold energy to generate optical breakdown is  $E_{Th} = 2.23$  nJ. Optical breakdown was associated with a density of generated free electrons exceeding  $\rho_{Bd} = 10^{21} \text{ cm}^{-3}$ . The threshold energy obtained numerically is in good agreement with experimental data [19]. Heisterkamp et al. reported a threshold energy of  $E = 2.2$  nJ in fixated cells, using an oil immersion objective ( $NA = 1.4$ ),  $\lambda = 790$  nm, and pulse duration 200 – 250 fs.

Fig. (4) shows optical breakdown plasmas calculated for varying numerical aperture ( $0.5 \leq NA \leq 1.2$ ). Pulse energies were chosen to be 5 % above threshold for optical breakdown, pulses were incident from the left, the geometrical focus is located at  $z = 0$ , and areas where the breakdown plasma density is exceeded ( $\rho > \rho_{Bd}$ ) are colored white. For the lowest numerical aperture considered ( $NA = 0.5$ ) a distinctive asymmetry of the generated plasma along the propagation direction is clearly observable. The highest plasma density is obtained some micrometers before the geometrical focus. Nonetheless, the plasma extends distinctively to the other side of the geometrical focus. This streak-like distortion of generated breakdown plasmas, found for  $NA < 0.9$  in fig. (4), is due to plasma-defocusing [15]. Streak formation was observed before at moderate focusing in various materials [12, 15 – 17]. However, for  $NA > 0.9$  axially symmetric breakdown plasmas, almost undistorted by plasma defocusing, with the highest plasma density generated in the geometrical focus are found.



**Fig. 4** Contour plots of optical breakdown plasmas calculated for varying numerical aperture ( $0.5 \leq NA \leq 1.2$ ) are shown. The pulse energy was chosen 5 % above the threshold for each NA. The isocontour lines are at the levels  $\rho = 10^{19}, 10^{20}, 5 \times 10^{20} \text{ cm}^{-3}$ . The size of the numerical box strongly scales with the NA; no calculation was performed in shaded areas.

The threshold energy for optical breakdown rapidly increases as the numerical aperture decreases (fig. 5). For  $NA \geq 0.9$  this increase scales well with the transverse focal spot size ( $A_{Focus} \sim 1/NA^2$ ). For  $NA < 0.9$  the pulse energy deviates strongly from this simple assumption. There are two basic reasons for the deviation observed. Firstly, as the NA decreases the focal volume expands even faster ( $V_{Plasma} \sim 1/NA^4$ ) than the transversal spot size. The generation of optical breakdown is not limited to the focal plane, but the plasma expands along the optical axis. Secondly, parasitic effects additionally enlarge the size of the plasma and thus the threshold pulse energy.



**Fig. 5** The graph shows the threshold pulse energy for optical breakdown vs. the numerical aperture. The red points indicate the common assumption that optical breakdown is limited to the focal plane and the pulse energy thus scales with the transversal focal spot size ( $A_{Focus} \sim 1/NA^2$ ).

The most common ultrashort pulse emitting lasers used in applications of cell surgery and nanoprocessing of materials are based on Titanium:Sapphire at wavelength of about 780 – 800 nm. However, recently also ultrashort pulse lasers based on ytterbium doped crystals and fibers were used in similar applications. Due to direct diode-

pumping this type of lasers is generally simpler and cheaper as compared to Ti:Saph-based lasers. The wavelength is around 1040 nm and the pulse duration is typically longer  $\tau > 250$  fs (FWHM).

Fig. (6) shows plasmas generated at the threshold for optical breakdown for four different wavelengths at NA = 1.2. For the sake of simplicity the pulse duration was chosen to be 150 fs (FWHM) for all wavelengths here. Additionally to 780 nm also a wavelength of 700 nm was chosen, which is about the lower limit of the tuning range of Ti:Saph lasers. The nonlinear order of multiphoton ionization is reduced from 5 to 4 when the wavelength is changed from 780 nm to 700 nm. For Yt-based lasers the second harmonic at 520 nm is also considered. The key parameters to compare the precision achievable at different wavelengths are the size and the energy of the generated plasmas. Although the threshold pulse energy is lower for 700 nm, it can be observed from fig. (6) that precision apparently cannot be enhanced by tuning the wavelength from 780 nm to 700 nm for Ti:Saph lasers. On the other hand, using the second harmonic for Yt-based lasers, the generated plasma is much smaller and the plasma energy is about four times lower as compared to the fundamental wavelength. The plasma energy is found lowest at 520 nm for all four wavelengths compared ( $E_{\text{Plasma, 520 nm}} = 22$  pJ).

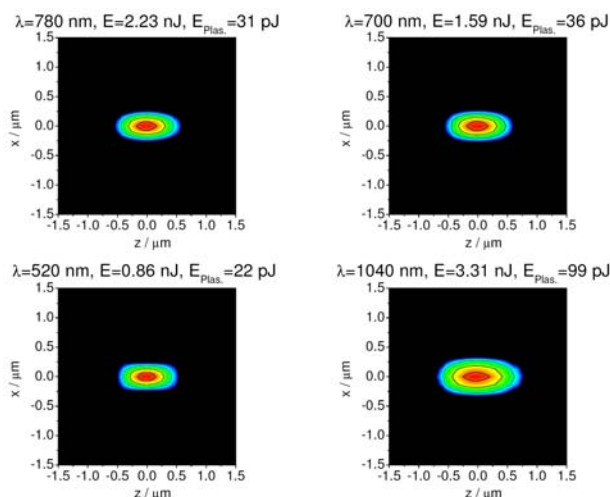


**Fig. 6** Plasmas generated at NA = 1.2 for different wavelengths at threshold energy and pulse duration 150 fs (FWHM).

Following the assumptions of Vogel et al. [33] the maximum size of the resulting cavitation bubble can be estimated from the energy of the generated Plasma. For the plasma generated at 780 nm in fig. 6 the bubble energy and radius can be estimated to  $E_{\text{Cav.}} \approx 10$  fJ and  $R_{\text{Cav.}} = 300$ -400 nm, respectively. This is in agreement with values found by Vogel et al. at the threshold for optical breakdown [33, 40].

Finally the dependence of the optical breakdown threshold energy was studied as a function of the pulse duration (fig. 7). The threshold on the surface of a material is generally expected to continuously decrease as the pulse duration is decreased [41 - 43]. This characteristic behaviour is well reproduced by solving the ionization model without propagation, as shown by the continuous line in fig. (7). However, the threshold energy inside the medium can be quite different, especially at low NA when parasitic

effects are strong. This can be observed from the dotted curve in fig. (7), indicating the modelled threshold energy for NA = 0.5 within the volume of water. Surprisingly the threshold inside the medium features a distinct minimum at about 200 fs. For shorter pulse duration the threshold rapidly increases. For longer pulse duration the threshold increases much slower as compared to the surface. Hence for specific applications it can be favourable not to use the shortest pulse available, in order to generate the smallest material alterations. Similar behaviour was also presented experimentally by Burakov et al., when structuring the bulk of fused silica at NA = 0.45 [17]. In that work modifications to the bulk of the material were found to be much smaller and better localised around the geometrical focus using a pulse duration of 2 ps instead of 120 fs.

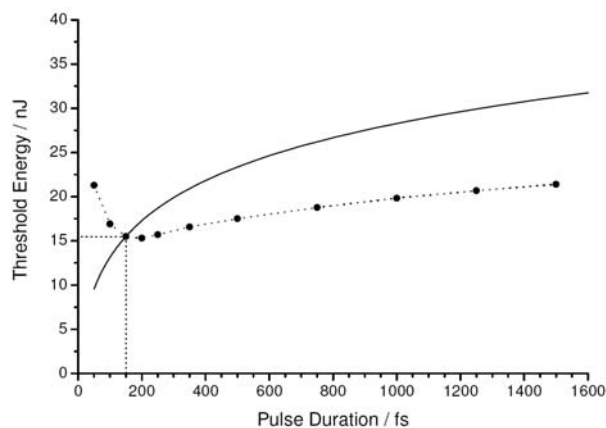


**Fig. 7** Threshold energy as a function of pulse duration for NA = 0.5 at the surface (continuous line) and inside the material (dotted line).

#### 4. Conclusion

The generation of optical breakdown at high numerical aperture was numerically studied taking into account nonlinear propagation and plasma formation. The theoretical model is based on a unidirectional, nonlinear propagation equation, derived from the vectorial Helmholtz equation. Unlike typical propagation equations the equation presented is not limited to the paraxial approximation, but particularly takes into account nonparaxiality and vectorial effects. The theoretical model was presented in detail in an earlier publication [1].

Using water as model substance for biological cells, optical breakdown plasmas were numerically studied as function of the pulse energy, the numerical aperture of the focusing optics, the wavelength, as well as the pulse duration. It was found that the parasitic side-effect of streak-formation is not a phenomenon limited to loose focusing, but can also be observed for relatively high numerical aperture. Breakdown plasmas, distinctively distorted in shape and size, were found for  $NA < 0.9$ . On the other hand, almost undistorted, symmetric breakdown plasmas of sub-diffraction size can be obtained for  $NA \geq 0.9$ , perfectly suited for minimum-invasive, intra-cellular dissection.

The size and energy of generated plasmas at the threshold for optical breakdown was studied for four different wavelengths. The smallest plasma with the lowest plasma energy was found for the second harmonic wavelength

(520 nm) of Yt-based lasers. The plasma energy at the fundamental wavelength was more than four times greater, indicating that using the second harmonic instead of the fundamental for Yt-based lasers could greatly increase the precision experimentally achievable. On the other hand, tuning the center wavelength from 780 nm to 700 nm for Ti:Sa-based lasers did not show an increase in precision.

For focusing conditions of low numerical aperture, when parasitic side-effects such as self-focusing, plasma defocusing, and streak formation strongly influence the generation of optical breakdown, pulses of longer pulse duration can be beneficial to generate smaller and better confined material alterations in a particular application.

## References

- [1] C. L. Arnold, A. Heisterkamp, W. Ertmer, and H. Lubatschowski: *Opt. Express*, 15, (2007) 10303.
- [2] B. Rethfeld: *Phys. Rev. Lett.*, 92, (2004) 187401.
- [3] R. Osellame, S. Taccheo, M. Marangoni, R. Ramponi, P. Laporta, D. Polli, S. De Silvestri, and G. Grullo: *J. Opt. Soc. Am. B*, 20, (2003). 1559.
- [4] Y. Lai, K. Zhou, L. Zhang, and I. Bennion: *Opt. Lett.*, 31, (2006) 2559.
- [5] T. Juhasz, F. H. Loesel, R. N. Kurtz, C. Horvath, J. F. Bille, and G. Mourou: *IEEE Sel. Top. Quantum Electron.*, 5, (1999) 902.
- [6] H. Lubatschowski, G. Maatz, A. Heisterkamp, U. Hetzel, W. Drommer, H. Welling, and W. Ertmer: *Graef. Arch. Clin. Exp.*, 238, (2000) 33.
- [7] K. König, I. Riemann, and W. Fritzsche: *Opt. Lett.*, 26, (2001) 819.
- [8] M. F. Yanik, H. Cinar, A. D. Chisholm, Y. Jin, and A. Ben-Yakar: *Nature* 432, (2004) 822.
- [9] I. Maxwell, S. Chung, and E. Mazur: *Med. Laser Appl.*, 20, (2005) 193.
- [10] S. H. Chung, D. A. Clark, C. V. Gabel, E. Mazur, and A. D. Samuel: *BMC Neuroscience*, 7, (2006).
- [11] S. M. Eaton, H. Zhang, P. R. Herman, F. Yoshino, L. Shah, J. Bovatsek, and A. Y. Arai: *Opt. Express*, 13, (2005) 4708.
- [12] L. Sudrie, A. Couairon, M. Franco, B. Lamouroux, B. Prade, S. Tzortzakis, and A. Mysyrowicz: *Phys. Rev. Lett.*, 89, (2002) 186601.
- [13] N. T. Nguyen, A. Saliminia, W. Liu, S. L. Chin, and R. Vallée: *Opt. Lett.*, 28, (2003) 1591.
- [14] J. B. Ashcom, R. R. Gattass, C. B. Schaffer, and E. Mazur: *Opt. Express*, 23, (2006) 2317.
- [15] C. L. Arnold, A. Heisterkamp, W. Ertmer, and H. Lubatschowski: *Appl. Phys. B*, 80, (2005) 247.
- [16] A. Couairon, L. Sudrie, M. Franco, B. Prade, and A. Mysyrowicz: *Phys. Rev. B*, 71, (2005) 125435.
- [17] I. M. Burakov, N. M. Bulgakova, R. Stoian, A. Mermillod-Blondin, E. Audouard, A. Rosenfeld, A. Husakou, and I. V. Hertel: *J. Appl. Phys.*, 101, (2007) 043506.
- [18] A. Heisterkamp, T. Ripken, T. Mamom, W. Drommer, H. Welling, W. Ertmer, and H. Lubatschowski: *Appl. Phys. B*, 74, (2002) 419.
- [19] A. Heisterkamp, I. Z. Maxwell, and E. Mazur: *Opt. Express*, 13, (2005) 3690.
- [20] Q. Feng, J. V. Moloney, A. C. Newell, E. M. Wright, K. Cook, P. K. Kennedy, D. X. Hammer, B. A. Rockwell, and C. R. Thompson: *IEEE J. Quantum. Electron.*, 33, (1997) 127.
- [21] A. Dubietis, A. Couairon, E. Kucinskas, G. Tamosauskas, E. Gaizauskas, D. Faccio, and P. Di Trapani: *Appl. Phys. B*, 84, (2006) 439.
- [22] M. Kolesik and J. V. Moloney: *Phys. Rev. E*, 70, (2004) 036604.
- [23] M. D. Feit and J. Fleck, Jr.: *J. Opt. Soc. Am. B*, 5, (1988) 633.
- [24] N. Akhmediev, A. Ankiewicz, and J. M. Soto-Crespo: *Opt. Lett.*, 18, (1993) 411.
- [25] G. Fibich and B. Ilan: *Physica D* 157, (2001) 112.
- [26] M. Kolesik, J. V. Moloney, and M. Mlejnek: *Phys. Rev. Lett.*, 89, (2002) 283902.
- [27] J. H. Marburger: *Prog. Quant. Electr.*, 4, (1975) 35.
- [28] B. Richards and E. Wolf: *Proc. R. Soc. A*, 253, (1959).
- [29] Y. M. Engelberg and S. Ruschin: *J. Opt. Soc. Am. A*, 21, (2004) 2135.
- [30] M. Gu: "Advanced Optical Imaging Theory", (Springer, Berlin, 2000).
- [31] F. Docchio, C.A. Sachhi, J. Marshall, *Lasers Ophthalmol.*, 1, (1986) 83.
- [32] F. Williams, S. P. Varma, and S. Hillenius: *J. Chem. Phys.*, 64, (1976) 1549.
- [33] A. Vogel, J. Noack, G. Hüttman, and G. Paltauf: *Appl. Phys. B*, 81, (2005) 1015.
- [34] S. Chi and Q. Guo: *Opt. Lett.*, 20, (1995) 1598.
- [35] P. K. Kennedy: *IEEE J. Quantum. Electron.*, 31, (1995) 2241.
- [36] B. C. Stuart, M. D. Feit, A. M. Rubenchik, B. Shore, and M. D. Perry: *Phys. Rev. Lett.*, 74, (1995) 2248.
- [37] A. Kaiser, B. Rethfeld, M. Vicanek, and G. Simon: *Phys. Rev. B*, 61, (2000) 11437.
- [38] L. V. Keldysh: *Sov. Phys. JETP*, 20, (1965) 1307.
- [39] E. Wolf: *Proc. R. Soc. A*, 253, (1959) 349.
- [40] A. Vogel, N. Linz, S. Freidank, and G. Paltauf: *Phys. Rev. Lett.*, 100, (2008) 038102
- [41] B. C. Stuart, M. D. Feit, S. Herman, A. M. Rubenchik, B. W. Shore, M. D. Perry: *Phys. Rev. B*, 53, (1996) 1749.
- [42] M. Lenzner, J. Krüger, S. Sartania, Z. Cheng, C. Spielmann, G. Mourou, W. Kautek, F. Krausz: *Phys. Rev. Lett.*, 80, (1998) 4076.
- [43] A.-C. Tien, S. Backus, H. Kapteyn, M. Murnane, G. Mourou: *Phys. Rev. Lett.*, 82, (1999) 3883.

(Received: July 4, 2008, Accepted: March 2, 2009)